

MODÈLE DE CHAMP DE PHASE POUR L'ÉTUDE DE L'ENDOMMAGEMENT ET LA RUPTURE DANS LES MATÉRIAUX CRISTALLINS

Hela GMATI ^a, Charles MAREAU ^a, Amine AMMAR ^a, Saber EL AREM ^a

^a Arts et Métiers ParisTech, 2 Boulevard du Ronceray, BP 93525, F-49035 Angers cedex 01, France

Mots-clés : Fracture, Crack propagation, Phase-field, Finite element, Anisotropy.

Abstract

In the present work, a stress-based damage gradient model is developed to address the numerical simulation of brittle fracture. This model succeeds in capturing some important aspects of crack propagation including crack branching and bifurcation. Also, the proposed phase field model has been developed in the general framework of anisotropic elasticity. It can thus be used for the simulation of brittle fracture in polycrystalline materials, for which crack propagation is impacted by crystallographic orientation because of the anisotropic character of stiffness properties.

1 Introduction

Microstructure optimization requires a deep understanding of the influence of microstructural heterogeneities on damage development. The description of damage through computational models is therefore an important challenge in material science. However, the incorporation of damage in constitutive models is a complex task, mostly because of the computational issues associated with the nucleation and propagation of discontinuity surfaces (i.e. cracks). Those difficulties can be circumvented with the Phase-Field Method (PFM), which provides a general framework for treating moving boundary problems.

Though the PFM has originally been applied to phase transition problems [5], the application of the PFM to damage problems has recently received much attention. For instance, based on the variational approach developed by Francfort and Marigo [3], Bourdin et al. [2] have proposed a model for the description of brittle fracture. Also, a robust formulation, based on continuum mechanics and thermodynamics, has been presented by Miehe et al. [8, 7]. In the later, particular care has been taken to account for the closure effects governing tension-compression asymmetry. This approach has been used by Nguyen et al. [9] to model the behavior of cementitious materials. The works of Larsen [6], Bourdin et al. [2], Borden et al. [1], and Hofacker and Miehe [4] have shown that the PFM can be extended to dynamic fracture and produce results that agree properly with experimental observations. The above models based on the PFM are smooth continuum formulations which do not require an explicit tracking of discontinuity surfaces. As a result, the main advantage of this method is its ability to produce complex crack patterns, including branching and merging, in both two and three dimensions. This work aims at developing a constitutive model within the general framework of the PFM to deal with damage propagation in polycrystalline materials. More specifically, a non-local damage model, which considers a scalar damage variable and its gradient as state variables, is constructed. The proposed model is adapted to any class of material symmetry and particular care is taken to differentiate the effects of positive and negative stresses on the development of damage. The present paper is organized as follows. The first section is dedicated to the description of the proposed constitutive model. For illustration purposes, the impact of elastic anisotropy, which can be significant for crystalline materials, is investigated in the second section.

2 Model description

2.1 Field equations

In order to model the process driving the development of damage, the response of a volume element V with boundary ∂V is given by the evolution of a displacement (vector) field \mathbf{u} and a damage (scalar) field d , which

plays the role of an order parameter. The equilibrium equations are obtained from the application of the virtual work principle¹ :

$$\mathcal{P}_i = \mathcal{P}_e \quad (1)$$

With :

$$\mathcal{P}_i = \int_V (\boldsymbol{\sigma} : \nabla \otimes \delta \mathbf{u} + y \delta d + \boldsymbol{\eta} \cdot \nabla \delta d) dV \quad (2)$$

$$\mathcal{P}_e = \int_V \mathbf{b} \cdot \delta \mathbf{u} dV + \int_{\partial V} \mathbf{t} \cdot \delta \mathbf{u} dS \quad (3)$$

where $\boldsymbol{\sigma}$ is the Cauchy stress tensor. The driving force associated with d is denoted by y while the driving force associated with ∇d is $\boldsymbol{\eta}$. \mathbf{b} and \mathbf{t} are respectively the volume and surface force densities. The application of the virtual work principle leads to the following mechanical equilibrium conditions and boundary conditions :

$$\boldsymbol{\sigma} \cdot \nabla + \mathbf{b} = \mathbf{0} \text{ in } V \quad (4)$$

$$\boldsymbol{\sigma} \cdot \mathbf{n} = \mathbf{t} \text{ in } \partial V \quad (5)$$

Also, the forces $\boldsymbol{\eta}$ and y must satisfy the following equilibrium conditions and boundary conditions :

$$y - \boldsymbol{\eta} \cdot \nabla = 0 \text{ in } V \quad (6)$$

$$\boldsymbol{\eta} \cdot \mathbf{n} = 0 \text{ in } \partial V \quad (7)$$

2.2 Constitutive relations

To describe the evolution of the displacement and damage fields, some constitutive relations are needed. To this end, the Gibbs free energy is chosen as a state potential and the Gibbs free energy density g is introduced. The free energy density g is decomposed into volume ψ and surface γ contributions :

$$g(\boldsymbol{\sigma}, d, \nabla d) = \psi(\boldsymbol{\sigma}, d) + \gamma(d, \nabla d) \quad (8)$$

The surface contribution takes the form :

$$\gamma(d, \nabla d) = \frac{g_c}{2l_c} d^2 + \frac{g_c l_c}{2} \nabla d \cdot \nabla d \quad (9)$$

where g_c is the cracked surface energy density and l_c is an internal length scale. For the volume contribution, the following decomposition is adopted :

$$\psi(\boldsymbol{\sigma}, d) = \psi^0(\boldsymbol{\sigma}) + c(d)(\psi^+(\boldsymbol{\sigma}) + A\psi^-(\boldsymbol{\sigma}) + B\psi^{+/-}(\boldsymbol{\sigma})) \quad (10)$$

With :

$$\begin{aligned} \psi^0(\boldsymbol{\sigma}) &= -\frac{1}{2} \boldsymbol{\sigma} : \mathbb{S}^0 : \boldsymbol{\sigma} \\ \psi^+(\boldsymbol{\sigma}) &= -\frac{1}{2} \boldsymbol{\sigma}^+ : \mathbb{S}^0 : \boldsymbol{\sigma}^+ \\ \psi^-(\boldsymbol{\sigma}) &= -\frac{1}{2} \boldsymbol{\sigma}^- : \mathbb{S}^0 : \boldsymbol{\sigma}^- \\ \psi^{+/-}(\boldsymbol{\sigma}) &= -\boldsymbol{\sigma}^- : \mathbb{S}^0 : \boldsymbol{\sigma}^+ \end{aligned} \quad (11)$$

where \mathbb{S}^0 denotes the initial (i.e. undamaged) elastic compliance tensor and $\boldsymbol{\sigma}^+$ (respectively $\boldsymbol{\sigma}^-$) represents the positive (respectively negative) stress tensor. A and B are two material parameters controlling tension/compression asymmetry. The monotonically increasing function $c(d) = d(2-d)/(1-d)^2$ is chosen to ensure the stiffness to vanish completely for a fully damaged (i.e. $d = 1$) material point :

$$c(0) = 0 \text{ and } c(1) = \infty \quad (12)$$

It should be noticed that the above formulation does not require any assumption regarding material symmetry.

1. In the present work, inertia effects are neglected.

The evolution relations associated with the different variables are obtained from a dissipation potential ϕ which depends on \dot{d} and d according to :

$$\phi(\dot{d}, d) = \begin{cases} \frac{K}{N+1} \frac{\dot{d}^{N+1}}{(1-d)}, & \dot{d} \geq 0 \\ \infty, & \dot{d} < 0 \end{cases} \quad (13)$$

where K and N are material parameters. The resistance to damage growth is controlled with K while the rate-sensitive character of damage development is adjusted with N . Using the expressions (8) and (13) of the state and dissipation potentials as well as the equilibrium condition (6), the equation governing the growth of damage is :

$$\langle -c'(\psi^+ + A\psi^- + B\psi^{+/-}) - \frac{g_c}{l_c}d + g_c l_c \Delta d \rangle (1-d) = K\dot{d}^N \quad (14)$$

where :

$$c' = \frac{2}{(1-d)^3} \quad (15)$$

Also, the infinitesimal strain tensor $\epsilon = \text{sym}(\nabla \otimes \mathbf{u})$ for each material point is obtained from the stress tensor σ according to :

$$\epsilon = \mathbb{S} : \sigma \quad (16)$$

with :

$$\mathbb{S} = \mathbb{S}^0 + c(d) \left(\frac{\partial \sigma^+}{\partial \sigma} : \mathbb{S}^0 : \left(\frac{\partial \sigma^+}{\partial \sigma} + B \frac{\partial \sigma^-}{\partial \sigma} \right) + \frac{\partial \sigma^-}{\partial \sigma} : \mathbb{S}^0 : \left(A \frac{\partial \sigma^-}{\partial \sigma} + B \frac{\partial \sigma^+}{\partial \sigma} \right) \right) \quad (17)$$

At the current stage, the dissipation potential (13) does not depend on the stress tensor σ . As a result, no inelastic type of deformation mechanism is considered. Future work will therefore have to focus on the incorporation of more complex phenomena (e.g. plasticity, hardening).

3 An illustrative example : A polycrystalline volume element under tension

In this section, for illustration purposes, the development of damage in a polycrystalline volume element under plane strain conditions is investigated. As shown in Figure 1, the volume element is a square plate of length 1mm containing a circular hole of radius $r = 0.04$ mm. The polycrystalline microstructure has been generated with a Voronoi tessellation of 60 seed points. The crystallographic orientations of the individual grains were assigned randomly. Here, only the specific case of cubic symmetry is considered. In this case, the initial fourth-rank stiffness tensor \mathbb{C}_0 has only three independent parameters C_{11} , C_{12} and C_{44} . Using Voigt notation for two dimensions, such a tensor can be written as

$$[\mathbb{C}_0] = \begin{pmatrix} C_{11} & C_{12} & 0 \\ C_{12} & C_{11} & 0 \\ 0 & 0 & C_{44} \end{pmatrix} \quad (18)$$

For the resolution of the differential equations resulting from static equilibrium and compatibility conditions, the explicit finite element method is used. For this purpose, the volume element is meshed with 105,582 triangular elements (see Figure 1). The typical size h of an element is about 2×10^{-3} mm in the crack propagation zone and 10^{-2} mm in the rest of the domain. The condition $4h \leq l_c$ [8] is therefore met in the crack propagation zone. The boundary conditions consist of imposing a progressive vertical displacement up to 0.06 mm to both the top and bottom edges. The simulation, whose duration is 1s, is decomposed into 20000 load increments.

		1	2	3	4	5
Elasticity	C_{11} [kN/mm ²]	180	180	156	95	52
	C_{12} [kN/mm ²]	104	100	87	53	29
	C_{44} [kN/mm ²]	21	40	69	105	117
	$\ C_0\ $ [kN/mm ²]	420	420	420	420	420
	Z	0.5	1	2	5	10
Damage	g_c [kN/mm]	2.7×10^{-3}				
	l_c [mm]	10^{-2}				
	A	10^{-3}				
	B	10^{-3}				

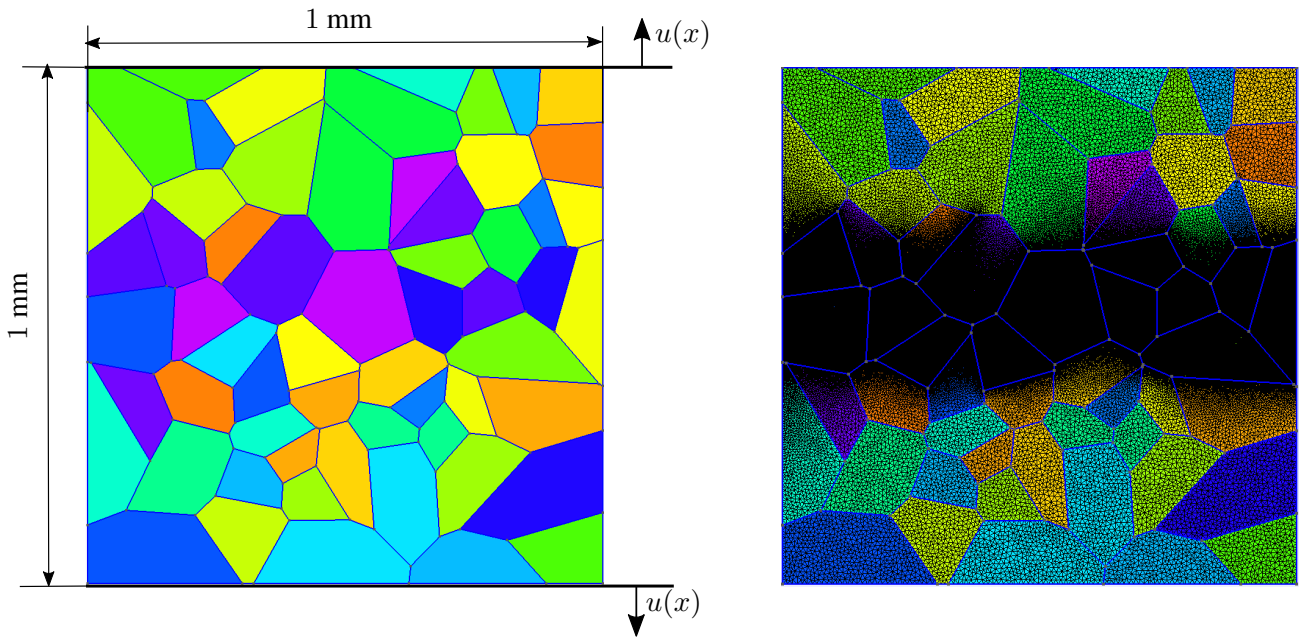
TABLE 1 – Material parameters for different Z values.

FIGURE 1 – Polycrystalline microstructure generated from a Voronoi tessellation of 60 randomly distributed seed points. Each color represents a random crystallographic orientation.

In order to evaluate the impact of elastic anisotropy on crack propagation, some simulations have been performed with different anisotropy factor. According to Zener [10], the anisotropy factor for cubic crystals is given by :

$$Z = 2(C_{11} - C_{12})/C_{44} \quad (19)$$

As illustrated by Table 1, the anisotropy factor Z has been varied from 0, 5 to 10 in the present work. The specific case of isotropy corresponds to $Z = 1$. The load-displacement curves are shown in figure 3. Whatever the value of Z is, the load completely vanishes when the crack passes through the whole volume element. As shown in figure 2, the crack propagation path is impacted by elastic anisotropy. More specifically, in the isotropic case, the crack follows a straight line as the impact of microstructural heterogeneities is inexistant. At the opposite, when Z is very different from unity, some important deviations along the crack propagation path are observed. Also, for the case where Z is equal to 10, the important internal stresses around a triple junction are responsible for a branching phenomenon.

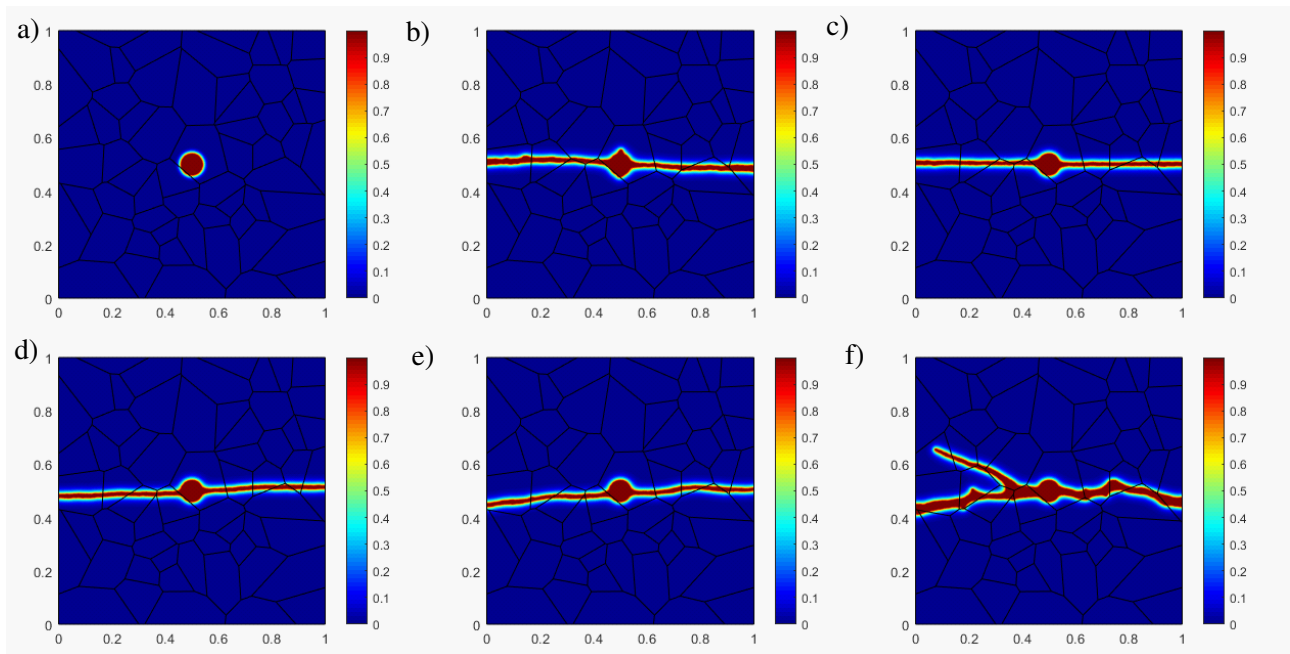


FIGURE 2 – Evolution of the damage phase field in a polycrystalline patch subjected to a tension test a) Initial volume element with a void situated in the middle of the plate b) $Z = 0.5$, c) $Z = 1$, d) $Z = 2$, e) $Z = 5$ and f) $Z = 10$

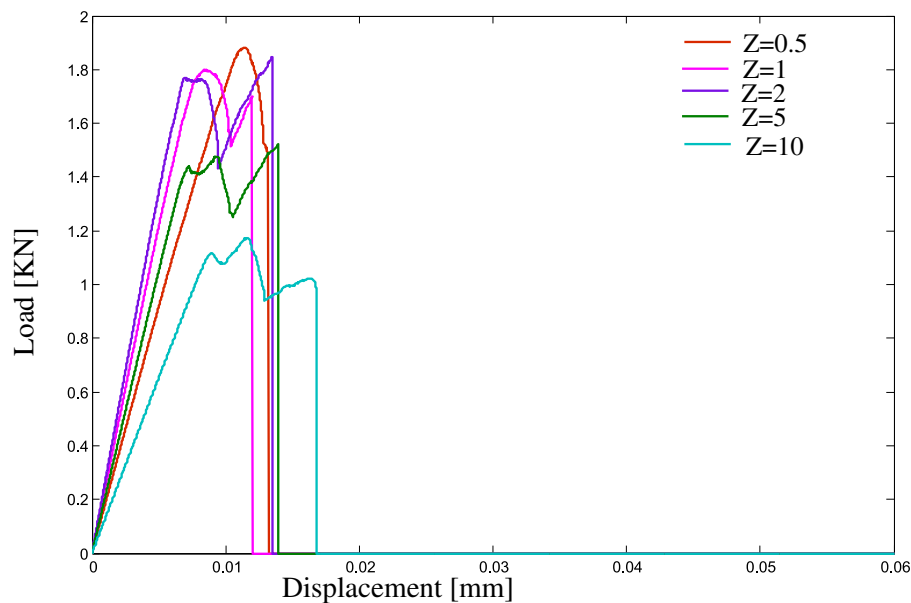


FIGURE 3 – Load-displacement curves for the polycrystalline patch subjected to a tension test for different Zener coefficients.

4 Conclusion

The present work aims at using the PFM to describe the development of damage in polycrystalline materials. The advantages of the PFM relies in its ability to treat the development of damage in a smooth fashion, which facilitates the numerical treatment of the problem. However, some additional developments are needed. Indeed, in the future, it will be necessary to describe more complex phenomena such as plasticity and hardening. Future work will thus focus on the construction of a model which includes the role of damage on plasticity and hardening.

Also, an important part of this work will be dedicated to the validation of the proposed model. It will thus be necessary to imagine some case studies to evaluate the limitations of the model.

Références

- [1] M. J. Borden, C. V. Verhoosel, M. A. Scott, T. J. Hughes, and C. M. Landis. *A phase-field description of dynamic brittle fracture*. *Computer Methods in Applied Mechanics and Engineering*, 217(22) :77 – 95, 2012.
- [2] B. Bourdin, C. J. Larsen, and C. L. Richardson. *A time-discrete model for dynamic fracture based on crack regularization*. *International Journal of Fracture*, 168(2) :133–143, 2011.
- [3] G. Francfort and J.-J. Marigo. *Revisiting brittle fracture as an energy minimization problem*. *Journal of the Mechanics and Physics of Solids*, 46(8) :1319 – 1342, 1998.
- [4] M. Hofacker and C. Miehe. *A phase field model of dynamic fracture : Robust field updates for the analysis of complex crack patterns*. *International Journal for Numerical Methods in Engineering*, 93(3) :276–301, 2013.
- [5] A. Karma. *Phase-field formulation for quantitative modeling of alloy solidification*. *Phys. Rev. Lett.*, 87 :115701, Aug 2001.
- [6] C. J. Larsen. *Models for Dynamic Fracture Based on Griffith’s Criterion*, pages 131–140. *Springer Netherlands, Dordrecht*, 2010.
- [7] C. Miehe, M. Hofacker, and F. Welschinger. *A phase field model for rate-independent crack propagation : Robust algorithmic implementation based on operator splits*. *Computer Methods in Applied Mechanics and Engineering*, 199(45) :2765 – 2778, 2010.
- [8] C. Miehe, F. Welschinger, and M. Hofacker. *Thermodynamically consistent phase-field models of fracture : Variational principles and multi-field fe implementations*. *International Journal for Numerical Methods in Engineering*, 83(10) :1273–1311, 2010.
- [9] T. nguyen, J. Yvonnet, Q.-Z. Zhu, M. Bornert, and C. Chateau. *A phase field method to simulate crack nucleation and propagation in strongly heterogeneous materials from direct imaging of their microstructure*. *Engineering Fracture Mechanics*, 139 :18–39, 2015.
- [10] C. M. Zener and S. Siegel. *Elasticity and anelasticity of metals*. *The Journal of Physical and Colloid Chemistry*, 53(9) :1468–1468, 1949.